Effects of quarks on the formation and evolution of Z(3) walls and strings in an effective model near the QCD deconfining transition

Uma Shankar Gupta,[1,*] Ranjita K. Mohapatra,[2,†] Ajit M. Srivastava,[2,‡] and Vivek K. Tiwari[1,§]

[1]*Physics Department, Allahabad University, Allahabad 211002, India*

[2]*Institute of Physics, Sachivalaya Marg, Bhubaneswer 751005, India*

(Received 13 November 2011; revised manuscript received 2 October 2012; published 6 December 2012)

We investigate the effects of explicit breaking of Z(3) symmetry due to the presence of dynamical quarks on the formation and evolution of Z(3) walls and associated quark-gluon plasma (QGP) strings within the Polyakov loop model. We carry out numerical simulations of the first order quark-hadron phase transition via bubble nucleation (which may be appropriate, for example, at finite baryon chemical potential) in the context of relativistic heavy-ion collision experiments. Using appropriate shifting of the order parameter in the Polyakov loop effective potential, we calculate the bubble profiles using the bounce technique for the true vacuum as well as for the metastable Z(3) vacua, and estimate the associated nucleation probabilities. These different bubbles are then nucleated and evolved, and the resulting formation and dynamics of Z(3) walls and QGP strings are studied. We discuss various implications of the existence of these Z(3) interfaces and the QGP strings, especially in view of the effects of the explicit breaking of the Z(3) symmetry on the formation and dynamical evolution of these objects.

DOI: 10.1103/PhysRevD.86.125016 PACS numbers: 25.75.−q, 11.27.+d, 12.38.Mh

I. INTRODUCTION

The possibility of the existence of topologically nontrivial structures such as Z(3) interfaces and associated quark-gluon plasma (QGP) strings in the quark-gluon plasma phase [1] is very exciting. In the context of relativistic heavy-ion collision experiments (RHICE), it provides the only system where domain walls and strings arise in a relativistic quantum field theory which can be investigated under laboratory control. In earlier works [1–3] we discussed various aspects of the existence of these objects in cosmology as well as in RHICE. These topological objects arise in the high temperature deconfined phase of QCD due to spontaneous breaking of the Z(3) global symmetry of finite temperature QCD, where Z(3) is the center of the $SU(3)$ color gauge group of QCD. Spontaneous breaking of Z(3) symmetry arises from the nonzero expectation value of the Polyakov loop, $l(x)$, which is an order parameter for the confinement-deconfinement (C-D) phase transition for pure gauge theory [4]. The interpolation of $l(x)$ between three different degenerate Z(3) vacua leads to the existence of domain walls (interfaces) together with topological strings when the three interfaces make a junction. We call these strings QGP strings [1].

The properties and physical consequences of these Z(3) interfaces have been discussed in the literature [5]. It has also been suggested that these interfaces should not be taken as physical objects in the Minkowski space [6]. The existence of these Z(3) vacua becomes especially a nontrivial issue when considering the presence of dynamical quarks. The effect of quarks on Z(3) symmetry and Z(3) interfaces, etc., has been discussed in detail in the literature [7,8]. It has been argued that the Z(3) symmetry becomes meaningless in the presence of quarks [7]. Another viewpoint as advocated in many papers asserts that one can take the effect of quarks in terms of explicit breaking of Z(3) symmetry [8–10], and we will follow this approach. In this context we mention the recent work of Deka *et al.* [11], which has provided support for the existence of these metastable vacua from lattice. Although the temperatures are high (close to 1 GeV) at which the indications of metastable vacuum are seen in Ref. [11], the important point is that these metastable Z(3) vacua seem to exist at some temperature. Since the presence of quarks lifts the degeneracy of different Z(3) vacua [8–10], the Z(3) interfaces become unstable and move away from the region with the unique true vacuum. Thus, with quark effects taken in terms of explicit symmetry breaking, the interfaces survive as nontrivial topological structures, though they do not remain solutions of time independent equations of motion. In our earlier investigations of these Z(3) walls and the QGP string, we neglected the effects of such an explicit symmetry breaking arising from quark effects [1–3], and investigated the properties and physical consequences of these objects Z(3) in the context of the early Universe as well as in RHICE. In the present work, we will incorporate effects of explicit symmetry breaking from quarks in the study of these objects.

Our numerical simulations in this work aim to investigate how the formation of Z(3) walls and string network during the initial C-D transition in RHICE, and how their subsequent evolution gets affected by such explicit breaking of Z(3) symmetry. As in our earlier works, we model the preequilibrium stage of phase transition in our

*guptausg@gmail.com
†ranjita@iopb.res.in
‡ajit@iopb.res.in
§vivek_krt@hotmail.com

simulation as a quasiequilibrium stage with an effective temperature which first rises (with rapid particle production) to a maximum temperature $T_0 > T_c$, where T_c is the critical transition temperature and then decreases due to continued expansion of plasma.

In order to study the C-D phase transition in earlier works for the pure gauge case, we have been using the mean field effective potential of a polynomial form written in terms of the Polyakov loop expectation value $l(x)$ as proposed by Pisarski [9,10]. A linear term in $l(x)$ added to this effective potential in the mean field framework [12–15] accounts for the explicit breaking of Z(3) symmetry by the dynamical quarks whose presence act like a background magnetic field [16]. In our analysis in Refs. [1,3] we discussed the effects of the explicit symmetry breaking term in view of the estimates of such a term from Ref. [17]. We found that the two degenerate vacua ($l = e^{i2\pi/3}$ and $l = e^{i4\pi/3}$), which get lifted with respect to the true vacuum (with $l = 1$) on account of explicit breaking of Z(3) symmetry in the QGP phase, have higher free energy than even the hadronic phase (with $l = 0$) at temperatures of order 200 MeV. This does not seem reasonable because one would expect that any of the Z(3) vacua which become metastable due to explicit symmetry breaking should still have lower free energy than the hadronic phase for values of temperature $T > T_c$ enforcing that the system lies in the deconfining regime for such temperatures. In any case, the estimates of Ignatius *et al*. [17] refer to high temperature regime and may not be applicable to temperatures near T_c. We thus use the following considerations to constrain the magnitude of the strength of the explicit symmetry breaking term. One approach can be to limit it such that the metastable vacuum remains lower than the confining vacuum for temperatures above T_c. We, however, limit explicit symmetry breaking to further lower values by requiring that the first order nature of the transition should remain at least in some range of temperatures above T_c.

We use this first order transition model in the present work to discuss the dynamical details of quark-hadron transition, even though the lattice results show that quark-hadron transition is most likely a crossover at zero chemical potential. The quark-hadron phase transition in the context of relativistic heavy-ion collision experiments is expected to be of first order for large values of the chemical potential which may be relevant for our study. Thus our study will be relevant for lower energy collisions which explore relatively high chemical potential regime of the QCD phase diagram. Further, we are primarily interested in determining the time dependence of Z(3) interfaces and string network structures, which result due to explicit breaking of Z(3) symmetry during the phase transition. The formation of these objects results from the simple fact that the correlation length remains finite in a fast evolving system, as shown by Kibble [18]. The distribution of these objects therefore shows universal features, independent of the details of the phase transition. The Kibble mechanism was first proposed for the formation of topological defects in the context of the early Universe [18], but it is now utilized extensively for discussing topological defects production in a wide variety of systems from condensed matter physics to cosmology [19]. The essential ingredient of the Kibble mechanism is the existence of uncorrelated domains of the order parameter which result after every phase transition occurring in finite time due to finite correlation length. A first order transition allows easy implementation of the resulting domain structure, especially when the transition proceeds via bubble nucleation. Keeping this view in mind, we use the potential for Polyakov loop augmented with the addition of a linear term as in Refs. [9,10] to model the phase transition. Further, we will be confining ourselves to the temperature/time ranges and such values of the coefficient of linear term in the effective potential that the first order quark-hadron transition proceeds via bubble nucleation.

The Z(3) interfaces and strings will develop dynamics in the presence of explicit symmetry breaking and the interfaces will start moving away from the direction where true vacuum exists. The strings will also not have three interfaces forming symmetrically around them, and hence will start moving in some direction. Such motions may cause important differences on the long time behavior. Due to the quark effects, we will get different nucleation probabilities/rates for the bubbles of metastable Z(3) vacua and the true vacuum bubbles of the QGP phase. Metastable bubbles being larger in size may cover a larger fraction of the physical space and hence may lead to nontrivial consequences. The effects of quarks will be significant if a closed spherical wall (with true vacuum inside) starts expanding instead of collapsing. This effect may play an important role in the early Universe case because an expanding closed domain wall has to be large enough such that the surface energy contribution does not dominate over the volume energy. In the case of RHICE, the asymmetrical Z(3) walls and associated strings will eventually melt away when the temperature drops below the deconfinement-confinement phase transition temperature T_c. However, they will be leaving their signatures in the form of extended regions of energy density fluctuations (as well as P_T enhancement of heavy-flavor hadrons [20]). We will be estimating these energy density fluctuations which will lead to multiplicity fluctuations. As in our earlier work [1], here also our main focus is looking for the signals of extended regions of large energy densities in space-time reconstruction of hadron density. We mention here that a simulation of spinodal decomposition in the Polyakov loop model has been carried out in Ref. [21], where fluctuations in the Polyakov loop are investigated in detail. Our work here and in Ref. [1] is focused on the formation of extended structures Z(3) walls, strings, and extended regions of energy density, etc., and in the present work how these are affected by effects of quarks.

The paper is organized in the following manner. In Sec. II, we briefly recall the Polyakov loop model of confinement-deconfinement phase transition and describe the effective potential proposed by Pisarski [9]. Here we discuss the effects of quarks in terms of a linear term in the Polyakov loop in the effective potential, which leads to explicit breaking of the Z(3) symmetry. We discuss different estimates for the strength of this linear term in the context of situations such that the transition is of first order. In Sec. III, we discuss the effect of this term on the structure of Z(3) walls and strings, and on the structure of bubbles through which the phase transition is completed. Here we describe our approach to extend the conventional technique of false vacuum decay to this case where different Z(3) bubbles have different profiles. What is of crucial importance to our discussion of the formation of these objects is the nucleation rates of the bubbles of different Z(3) vacua. Since these vacua are no more degenerate, the corresponding bubbles will in general have different nucleation rates. Section IV discusses nucleation rates for these different bubbles. One may expect that the metastable Z(3) vacua should be suppressed as the corresponding bubbles have larger actions. We discuss the very interesting possibility that despite having larger action, the metastable vacua may have similar (or even larger) nucleation rates as compared to the true vacuum. This can happen when the preexponential factor dominates over the exponential suppression term in the nucleation rate. This possibility is intriguing as the metastable vacua being larger in size may cover a larger fraction of the physical space and hence may dominate the dynamics of phase transition.

Section V presents the numerical technique of simulating the phase transition via random nucleation of bubbles, which now have different sizes depending on the corresponding Z(3) vacuum inside the bubble. The resulting domain walls may show nontrivial behavior compared to the case without the quark effects as a closed domain wall enclosing the true vacuum may expand instead of contract. Rough estimates with our parameter choices show that this is expected when the domain wall size exceeds about 50 fm. The discussion of such a large physical region is more relevant in the context of the early Universe and we plan to study this in a future work. Here we will consider the case relevant to RHICE with lattice sizes of about $(15\ \mathrm{fm})^2$ and study the effects of domain wall and string formation with temperature evolution as expected in a longitudinally expanding plasma. These results are presented in Sec. VI. We also calculate the energy density fluctuations associated with Z(3) wall network and strings, as in our earlier work [1], and discuss important differences for the present case with quark effects. In Sec. VII, we discuss possible experimental signatures resulting from the presence of Z(3) wall network and associate strings especially including the effects of explicit symmetry breaking. Section VIII presents our conclusions.

II. THE POLYAKOV LOOP MODEL WITH QUARK EFFECTS

We first briefly recall the Polyakov loop model for the confinement-deconfinement phase transition. For the case of pure $SU(N)$ gauge theory, the expectation value of Polyakov loop $l(x)$ is the order parameter for the confinement-deconfinement phase transition

$$l(\vec{x}) = \frac{1}{N}\,\mathrm{Tr}\left(\mathcal{P}\exp\left(ig\int_0^\beta A_0(\vec{x},\tau)d\tau\right)\right), \qquad (1)$$

where $A_0(\vec{x},\tau)$ is the time component of the vector potential $A_\mu(\vec{x},\tau) = A^a_\mu(\vec{x},\tau)T^a$, T^a are the generators of $SU(N)$ in the fundamental representation, $\mathcal{P}$ denotes path ordering in the Euclidean time τ, g is the gauge coupling, and $\beta = 1/T$ with T being the temperature. ($N = 3$ for QCD) is the number of colors. The complex scalar field $l(\vec{x})$ transforms under the global Z(N) (center) symmetry transformation as

$$l(\vec{x}) \longrightarrow \exp(2\pi i n/N) l(\vec{x}), \qquad n = 0, 1, \ldots (N-1). \qquad (2)$$

The expectation value of $l(x)$ is related to $e^{-\beta F}$ where F is the free energy of an infinitely heavy test quark. For temperatures below T_c in the confined phase, the expectation value of the Polyakov loop is zero corresponding to the infinite free energy of an isolated test quark. [Hereafter, we will use the same notation $l(x)$ to denote the expectation value of the Polyakov loop.] Hence the Z(N) symmetry is restored below T_c. Z(N) symmetry is broken spontaneously above T_c where $l(x)$ is nonzero corresponding to the finite free energy of the test quark. Effective theories of the Polyakov loop have been proposed by several authors with various parameters fitted to reproduce lattice results for pure QCD [9,10,22]. We use the Polyakov loop effective theory proposed by Pisarski [9,10]. The effective Lagrangian density can be written as

$$L = \frac{N}{g^2}|\partial_\mu l|^2 T^2 - V(l), \qquad (3)$$

where the effective potential $V(l)$ for the Polyakov loop in the case of pure gauge theory is given as

$$V(l) = \left(\frac{-b_2}{2}|l|^2 - \frac{b_3}{6}(l^3 + (l^*)^3) + \frac{1}{4}(|l|^2)^2\right)b_4 T^4. \qquad (4)$$

At low temperature where $l = 0$, the potential has only one minimum. As the temperature becomes higher than T_c the Polyakov loop develops a nonvanishing vacuum expectation value l_0, and the $\cos 3\theta$ term coming from the $l^3 + l^{*3}$ term above leads to Z(3) generate vacua. Now in the deconfined phase, for a small range of temperatures above T_c, the $l = 0$ extremum becomes the local minimum (false vacuum), and a potential barrier exists between the local minimum and global minimum (true vacuum) of the potential.

To include the effects of dynamical quarks, we follow the approach where the explicit breaking of the Z(3)

symmetry is represented in the effective potential by inclusion of a linear term in l [8–10,12]. The potential of Eq. (4) with the linear term becomes

$$V(l) = \left(-\frac{b_1}{2}(l + l^*) - \frac{b_2}{2}|l|^2 - \frac{b_3}{6}(l^3 + l^{*3}) + \frac{1}{4}(|l|^2)^2\right)b_4 T^4. \quad (5)$$

Here, coefficient b_1 measures the strength of explicit symmetry breaking. The coefficients b_1, b_2, b_3, and b_4 are dimensionless quantities. With $b_1 = 0$, the other parameters b_2, b_3, and b_4 are fitted in Refs. [9,10,23] such that the effective potential reproduces the thermodynamics of pure $SU(3)$ gauge theory on lattice [12,23,24]. The coefficient b_2 is temperature dependent and given by

$$b_2(r) = \left(1 - \frac{1.11}{r}\right)\left(1 + \frac{0.265}{r}\right)^2\left(1 + \frac{0.3}{r}\right)^3 - 0.487; \quad r = \frac{T}{T_c}; \qquad T_c = 182 \text{ MeV}.$$

We use the value of temperature independent coefficients $b_3 = 2.0$ and $b_4 = 0.6061 \times \frac{47.5}{16}$. We choose the same value of b_2 for real QCD (with three massless quarks flavors). b_4 is rescaled by factor $\frac{47.5}{16}$ to incorporate extra degrees of freedom of QCD relative to pure $SU(3)$ gauge theory [23]. As temperature $T \to \infty$ the Polyakov loop expectation value approaches the value $x \sim b_3/2 + \frac{1}{2}\sqrt{b_3^2 + 4b_2(T = \infty)}$. To have the normalization $\langle l(x)\rangle \to 1$ at $T \to \infty$, the coefficients and field in the effective potential $V(l)$ in Eq. (5) are rescaled as $b_1(T) \to b_1(T)/x^3$, $b_2(T) \to b_2(T)/x^2$, $b_3 \to b_3/x$, and $b_4 \to b_4 x^4$, $l \to l/x$.

At temperatures above the critical temperature T_c, the potential $V(l)$ has three degenerate vacua in pure gauge theory (with $b_1 = 0$). The barrier heights between the local minimum ($l(x) = 0$) and the three global minima ($l = 1$, z, z^2, corresponding to $\theta = 0, 2\pi/3, 4\pi/3$) are all the same. As the value of b_1 becomes nonzero, the degeneracy of Z(3) vacua gets lifted. Vacua corresponding to $\theta = 2\pi/3$ ($l = z$) and $\theta = 4\pi/3$ ($l = z^2$) remain degenerate, with energy which is higher than the $l = 1$ ($\theta = 0$) vacuum. Thus, $l = z$ and $l = z^2$ vacua become metastable and the $l = 1$ remains the only true vacuum (global minimum). Note that $l = z$ and $l = z^2$ are the two metastable vacua in the QGP phase. Along with these, there is a metastable vacuum at $l = 0$ (for a small range of temperatures above T_c) which corresponds to the confining phase.

Estimates of explicit Z(3) symmetry breaking arising from quark effects have been discussed in the literature. In the high temperature limit, the estimate of the difference in the potential energies of the $l = z$ vacuum and the $l = 1$ vacuum ΔV is given in Ref. [17] as

$$\Delta V \sim \frac{2}{3}\pi^2 T^4 \frac{N_l}{N^3}(N^2 - 2), \quad (6)$$

where N_l is the number of massless quarks. If we take $N_l = 2$ then $\Delta V \simeq 3T^4$. At $T = 200$ MeV, the difference between the confining vacuum and the true vacuum from the effective potential in Eq. (5) is about 150 MeV/fm^3 while ΔV from Eq. (6) at $T = 200$ MeV is about four times larger, equal to 600 MeV/fm^3. As T approaches T_c, this difference will become larger as the metastable vacuum and the stable vacuum become degenerate at T_c, while ΔV remains nonzero. It does not seem reasonable that at temperatures of order 200 MeV [with $T_c =$ 182 MeV for Eq. (5)], a QGP phase (with quarks) has higher free energy than the hadronic phase. In any case, the estimates of Eq. (6) were made in high temperature limit and the extrapolation of these to T near T_c may be invalid. We thus use different physical considerations to estimate the strength of the explicit symmetry breaking term; i.e., the value of parameter b_1 in Eq. (5) as follows.

Note that as b_1 is increased from zero, the potential tilts such that the barrier between the metastable confining phase and the true vacuum in the $\theta = 0$ direction decreases, resulting in the weakening of the first order phase transition. Finally, this barrier disappears for $b_1 \geq 0.11$ (at $T = T_c = 182$ MeV). For $b_1 \geq 0.11$ there is no range of temperatures where the phase transition is first order. As we mentioned, our approach is to study the phase transition dynamics via bubble nucleation. We thus choose a small value of $b_1 = 0.005$ such that the confinement-deconfinement phase transition is a (weakly) first order phase transition for a reasonable range of temperatures. The plot of the potential in $\theta = 0$ direction for $b_1 = 0.005$ is shown in Fig. 1 for $T = 200$ MeV. Note that with $b_1 > 0$ the confining vacuum at $l = 0$ shifts towards the positive real value of l. With this value of b_1, the barrier between the confining metastable vacuum and the true vacuum exists up to a temperature $\simeq 225$ MeV, which allows for a reasonable range of temperatures to discuss the bubble profiles and their nucleation probabilities. If we choose larger values of b_1, the range of temperatures allowing first order transition becomes very narrow, and the formation and nucleation of bubbles require fine-tuning of time scale.

This apparently *ad hoc* procedure of fixing the value of b_1 can be given a physical basis in the following way. Changing the value of coefficient b_1 changes the nature of the phase transition from a very strong first order to a very weak one. One can attempt to interpret it in the context of a QCD phase diagram drawn in the plane of chemical potential (μ) and temperature (T). The QCD phase transition is of strong first order for large μ; it becomes a weak first order transition with decreasing μ, reaches to its critical end point where the transition is of second order, and then becomes crossover at lower μ values. If we assume that the effective potential in Eq. (5) (at least in form) can describe these situations of

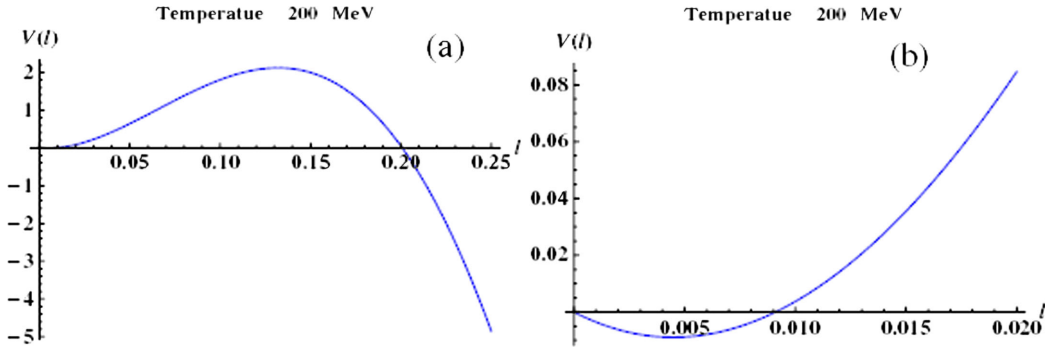

FIG. 1 (color online). (a) Plot of $V(l)$ (in MeV/fm^3) in the $\theta = 0$ direction for $T = 200$ MeV with $b_1 = 0.005$; (b) shows the plot near the origin showing that the confining vacuum has shifted slightly from $l = 0$ towards the $\theta = 0$ direction.

varying chemical potential, then it seems natural to assume that changing the value of μ is interpreted in terms of changing the value of the b_1 parameter in Eq. (5). Thus, increasing μ corresponds to lowering the value of b_1 making the phase transition of stronger first order.

Note that the potential barrier between the confining vacuum and the true vacuum is maximum when b_1 is zero, and the first order phase transition is strongest. This should correspond to the situation of largest μ according to the above argument, presumably corresponding to the transition at very low temperatures in the QCD phase diagram. However, with $b_1 = 0$ there is no explicit symmetry breaking. This will not be consistent with the expectation of explicit symmetry breaking arising from quark effects. Though one cannot exclude the possibility that the effects of dynamical quarks and that of net baryon number density may have opposite effects on the value of b_1 so that a strong first order transition at large μ can be consistently interpreted in terms of $b_1 = 0$. However, it is simpler to assume that even for the largest value of μ (where the first order curve intersects the μ axis in the QCD phase diagram), b_1 never becomes zero so that explicit symmetry breaking remains present as expected.

Of course, it is clear that the parameter values used in Eq. (5), which were fitted using lattice results for the $\mu = 0$ case, are no longer applicable if nonzero values of b_1 are interpreted in terms of nonzero μ. We will then need to assume that the required changes in the parameters of Eq. (5) for nonzero μ are not large. At the very least, we can say that even if the b_1 values we use here cannot be justified, they help us capture some qualitative aspects of changes in the formation and evolution of Z(3) walls and QGP strings when quark effects are incorporated.

III. DOMAIN WALLS, STRINGS, AND BUBBLES WITH EXPLICIT SYMMETRY BREAKING

The explicit symmetry breaking arising from quark effects will have important effects on the structure of topological objects: Z(3) walls and the QGP strings. It will obviously also affect the nucleation of bubbles of different Z(3) phases. First we qualitatively discuss its effects on Z(3) walls and the QGP strings. For nondegenerate vacua, even planar Z(3) interfaces do not remain static, and move away from the region with the unique true vacuum. Thus, while for the degenerate vacua case every closed domain wall collapses; for the nondegenerate case this is not true anymore. A closed wall enclosing the true vacuum may expand if it is large enough so that the surface energy contribution does not dominate. Similarly, it is no more possible to have a time independent solution for the QGP string. Without explicit symmetry breaking, a QGP string forming at the intersection of three symmetrically placed Z(3) walls will be stationary. However, with $b_1 \neq 0$ this is not possible for any configuration of domain walls. In fact, this type of situation has been discussed in the context of the early Universe for certain types of anionic string models [25].

Apart from the structure of these objects, one also expects important changes in the basic mechanism of the formation of these objects during the phase transition. Without explicit symmetry breaking, these objects will form via the Kibble mechanism, as discussed in detail in Ref. [1]. In the presence of explicit symmetry breaking, new effects may arise as discussed in Ref. [26] where many string-antistring pairs with small separations (which means small loops of strings or small closed domain walls in the present context) can form at the coalescence region of two bubbles. This mode of production of topological objects arises from the fluctuations of the order parameter, and it is entirely different from the basic physics of the Kibble mechanism. As we are using a very small value of explicit symmetry breaking we do not expect this new mechanism to play an important role here. However, for larger values of b_1, this production mechanism may play an important role in determining the Z(3) wall and string network resulting from a first order QCD phase transition.

A general picture of the formation of these objects during first order QCD transition via bubble nucleation was described in detail in Ref. [1] for the case without explicit symmetry breaking, and we briefly summarize it below. Subsequently, we will discuss the effects of explicit

symmetry breaking on the bubble profiles, their nucleation rates, and on the general dynamics of the phase transition.

We calculate the bubble profile of the QGP phase using Coleman's technique of bounce solution [27] for true vacuum ($l = 1$) and for metastable vacua ($l = z, z^2$). We seed these bubbles in the false (hadronic) background randomly with their nucleation rates calculated at an appropriate value of temperature $T > T_c$ (such that the nucleation rate is appreciable). The value of the phase of the complex order parameter l is constant inside a given bubble (to minimize the free energy), while it changes from one bubble to another randomly (corresponding to the choices of three vacua). The variation of the orientation of the order parameter from one bubble to another provides the essential ingredient of the Kibble mechanism leading to a domain structure and formation of topological objects at the intersection of domains. We evolve this initial field configuration with the equations of motion using a leapfrog algorithm. Bubbles grow with time and coalesce with each other. The bubbles with same vacuum merge together to form a bigger region of same vacuum while the bubbles with different vacua remain separated by a wall/interface of high energy density after coalescence. These are the Z(3) domain walls. These domain walls are the solutions of field equations of motion interpolating between different Z(3) vacua and survive for a very long time as QGP evolves. Eventually, either walls collapse/merge away, or they melt as the temperature of expanding QGP falls below T_c and Z(3) symmetry is restored.

Spontaneous breaking of Z(3) symmetry in the QGP phase leads to three different topological domain walls separating the three different Z(3) vacua. The intersection point of the three domain walls leads to a topological string (the *QGP* string) which was discussed in detail in Ref. [2]. This string arises as the order parameter l completes a closed loop around $l = 0$ in the complex l space when one encircles the intersection point of the three domain walls in the physical space [2]. Thus, these are topological strings which exist in the QGP phase and have confining core (with $l = 0$). As bubbles of different Z(3) vacua coalesce with each other, a network of Z(3) walls forms, and at the intersection of Z(3) walls, QGP strings form. A detailed investigation of this for the case without explicit symmetry breaking (i.e., $b_1 = 0$) using $2 + 1$ dimensional simulation representing the central rapidity region was carried out in Ref. [1].

The above picture of the dynamics of bubble nucleation, coalescence, and formation and evolution of Z(3) walls and QGP strings will be affected by the presence of explicit symmetry breaking in important ways. With $b_1 \neq 0$, the three Z(3) vacua are no longer degenerate. The two vacua ($l = z, z^2$) corresponding to $\theta = 2\pi/3, 4\pi/3$ get lifted and become metastable. Only the third one with a real expectation value of l remains stable. The energy difference between the confining vacuum (near $l = 0$, note that due to $b_1 \neq 0$, the confining vacuum shifts slightly) and the two metastable Z(3) vacua (with $l = z, z^2$) are smaller than the energy difference between the confining vacuum and the true vacuum. This leads to larger size for the bubble of metastable vacuum compared to the bubble of true vacuum. Consequently, the associated action (free energy) of the matastable vacuum bubble is also larger. The energy difference between the confining vacuum and the true or metastable vacuum increases with an increase in temperature, so the bubble sizes decrease with an increase in temperature.

In the nondegenerate case with nonvanishing explicit symmetry breaking, the false vacuum of potential gets shifted towards the real axis by a small amount ϵ. This shift is minimum for temperatures closer to T_c and increases as we increase the temperature. Further, the local maximum of the potential barrier and the metastable vacua are not in the same direction, but there is a small angular shift between them. These aspects make it difficult to apply the standard technique of finding the bounce solution for a scalar field for the present case as we will discuss below. First we review the basic features of the first order transition via bubble nucleation.

In a first order phase transition via bubble nucleation, a true vacuum bubble forms in the background of false vacuum. This bubble will grow or collapse depending on the free energy change of the system. The change in the free energy of the system because of the creation of a true vacuum bubble of radius R is

$$F(R) = F_s + F_v = 4\pi R^2 \sigma - \frac{4\pi}{3} R^3 \eta. \tag{7}$$

Here F_v is the volume energy, and F_s is the surface energy of the bubble. For a strong first order phase transition, one can analytically determine the potential energy difference η between the confining vacuum and relevant Z(3) vacuum and the surface tension σ from the bounce solution (at least for a scalar field). Minimization of this free energy determines the critical radius $R_c = \frac{2\sigma}{\eta}$. The volume energy of the bubbles with radius $R > R_c$ dominates over its surface energy, and the bubbles expand to transform the false vacuum to true vacuum. The smaller bubbles ($R < R_c$) for which surface energy dominates over the volume energy, shrink and disappear. For strong first order transition, the calculation of η and σ separately can be done as one is dealing with the thin wall bubbles where the bubble size is much larger than the thickness of the bubble wall, so that there is clear separation between the bubble core and the bubble wall. For the parameter values and the temperature range of our interest, we will be dealing with thick wall bubbles where the bubble size is of the same order as the bubble wall. For this purpose, the expression in Eq. (7) is not of use, and one has to calculate the bubble profile numerically using Coleman's technique of bounce solution and determine its action to calculate nucleation probabilities.

The theory of semiclassical decay of false vacuum at zero temperature is given in Ref. [27], and its extension to finite temperature was given in Ref. [28]. Coleman's technique is applicable for a real scalar field. To calculate the bubble profile for a complex scalar field l (with $b_1 = 0$) in Ref. [1], the phase angle θ was taken to be constant by fixing it in the direction of the relevant Z(3) vacuum, i.e., $\theta = 0, 2\pi/3$, or $4\pi/3$. This reduced the problem again to a real scalar field calculation and Coleman's technique could be directly applied. (However, there are important issues for the case of a complex scalar field regarding the calculation of nucleation rates which require the calculation of the determinant of fluctuations around the bounce solution. A brief discussion of these issues is provided in Ref. [1]).

We calculate the bubble profile in $3 + 1$ dimensions. However, we evolve it only by the $2 + 1$ dimensional field equations. This is because of a rapid longitudinal expansion which simply stretches the bubbles in the longitudinal direction, while its transverse evolution proceeds according to field equations. We neglect the transverse expansion of the system which is certainly a good approximation during the early stages of bubble nucleation (during the initial transition from the confining phase to the QGP phase with time scales of order 1 fm). At finite temperature, the $3 + 1$ dimensional theory will reduce to an effectively three-dimensional Euclidean theory if the temperature is sufficiently high, which we will take to be the case [1]. For this three-dimensional Euclidean theory, the bubble profile is the solution of the following equation:

$$\frac{d^2 l}{dr^2} + \frac{2}{r}\frac{dl}{dr} = \frac{g^2}{2NT^2}\frac{\partial V}{\partial l}, \tag{8}$$

where $r = r_E = \sqrt{\vec{x}^2 + t_E^2}$ and subscript E denotes coordinates in the three-dimensional Euclidean space. We use the fourth order Runge-Kutta method to solve Eq. (8). For $b_1 = 0$, the relevant boundary conditions on l to calculate the bubble profile are $l = 0$ as $r \to \infty$ and $\frac{dl}{dr} = 0$ at $r = 0$. However, with $b_1 > 0$ this is no longer applicable. This is because with $b_1 \neq 0$ the confining vacuum is shifted from $l = 0$ along the $\theta = 0$ direction by an amount ϵ. We calculate the bubble profile at $T = 200$ MeV and at this temperature $\epsilon = 0.0045$ [see Fig. 1(b)]. We thus rewrite the effective potential in Eq. (5) in terms of a shifted field $l' = l - \epsilon$. In terms of l', the confining vacuum again occurs at $l' = 0$, and the standard boundary conditions as discussed above can be applied for solving Eq. (8) for the bounce solution. Hereafter, all discussion will be in terms of this shifted field l', which for simplicity we will denote as l only.

Another complication occurs in calculating the bubble profile for the metastable Z(3) vacua. The earlier technique for the $b_1 = 0$ case of simply fixing $\theta = 2\pi/3$ or $\theta = 4\pi/3$ for the two respective vacua, thereby reducing the problem to a real scalar field case, cannot be applied here directly. This is because with $b_1 \neq 0$, the maximum of the respective potential barrier and the direction of the corresponding metastable vacuum are not in the same direction (due to the tilt of the potential resulting from $b_1 \neq 0$). However, the difference between the two directions, i.e., between the $l = z$ vacuum and the direction of the top of the corresponding barrier, is very small, of order $\theta = 0.9°$. The same is true for $l = z^2$ vacuum. We then fix θ along $l = z$ and $l = z^2$ vacua, respectively, to get the approximately valid bubble profile using Eq. (8). (Both of these directions differ slightly from $\theta = 2\pi/3$ and $\theta = 4\pi/3$ now. Note again all this is using the shifted field which we are again denoting as l). Recall that we are calculating the $3 + 1$ dimensional critical bubble and evolving it by $2 + 1$ dimensional equations with the bubble becoming supercritical for $2 + 1$ dimensional equations [1]. Further, we are studying the situation of rapidly changing temperature. Thus, the exact profile of the critical bubble at the nucleation time is not of much relevance.

As we mentioned above, we choose the value of b_1 such that the barrier between the confining vacuum and various Z(3) vacua remains nonzero up to some range of temperatures so that bubble formation can be carried out. We choose $b_1 = 0.005$ with which the barrier between the confining vacuum and true vacuum exist up to temperature $\simeq 225$ MeV. The first order phase transition via bubble nucleation is possible only up to this temperature.

IV. NUCLEATION RATES FOR DIFFERENT BUBBLES

For the finite temperature case, the tunneling probability per unit volume per unit time in the high temperature approximation is given by [28] (in natural units)

$$\Gamma = Ae^{-S_3(l)/T}, \tag{9}$$

where $S_3(l)$ is the three-dimensional Euclidean action for the Polyakov loop field configuration that satisfies the classical Euclidean equations of motion. The dominant contribution to the exponential term in Γ comes from the bounce solution which is the least action $O(3)$ symmetric solution of Eq. (8). For a theory with one real scalar field in three Euclidean dimensions, the preexponential factor arising in the nucleation rate of critical bubbles has been estimated, see Ref. [28]. The preexponential factor obtained from Ref. [28] for our case becomes

$$A = T^4\left(\frac{S_3(l)}{2\pi T}\right)^{3/2}. \tag{10}$$

As emphasized in Ref. [1], the results of Linde [28] were for a single real scalar field, and one of the crucial ingredients used in Ref. [28] for calculating the preexponential factor was the fact that for a bounce solution the only light modes contributing to the determinant of fluctuations were the deformations of the bubble perimeter. Even though we are discussing the case of a complex scalar field $l(x)$, this assumption may still hold as we are calculating the

tunneling from the false vacuum to one of the Z(3) vacua. This assumption may need to be revised when light modes (e.g., Goldstone bosons) are present which then also have to be accounted for in the calculation of the determinant.

A somewhat different approach for the preexponential factor in Eq. (9) is obtained from the nucleation rate of bubbles per unit volume for a liquid-gas phase transition as given in Refs. [29,30]. In Ref. [1], we considered these estimates for the nucleation rate as well as those obtained from Eq. (10). It was found that for the parameter values in Eq. (5) and for the temperature/time scales relevant for RHICE, the nucleation rates obtained using the liquid-gas transition approach of Refs. [29,30] were completely negligible such that even the nucleation of one bubble of the QGP phase was not likely in RHICE. As one needs several bubbles to discuss the formation of Z(3) walls and strings, these estimates clearly cannot be used here. As in Ref. [1], we will follow the approach based on Eq. (10) for our case which gave reasonable nucleation rates leading to the possibility of the formation of several bubbles for the case of RHICE. We may mention here that for the nucleation of bubbles of the Polyakov loop l, it may anyway be better to use a field theory approach as in Ref. [28], rather than the approach of Refs. [29,30] which is more suitable for the description of phase transition in terms of plasma degrees of freedom. Though the parameters of Eq. (5) have been fitted with lattice QCD, it is still not very clear whether the bubbles should be viewed in terms of an order parameter field representing some background condensate (as the Polyakov loop l), or just different phases of an interacting plasma.

We thus proceed with the calculation of nucleation rates of the bubbles, using Eqs. (9) and (10). Figure 2 shows the profiles of the bubbles for $l = 1$ and $l = z$ vacua at $T = 200$ MeV ($l = z^2$ bubbles have the same profile as the $l = z$ bubble). We note that the $l = z$ bubble is somewhat larger, as expected. Using such bubble profiles, we calculate the respective values of the action S_3 and estimate the nucleation rates for metastable and true vacuum at different temperatures. To calculate the number of bubbles for a typical nucleus-nucleus collision, we consider a circle of 8-fm radius in transverse plane with 1-fm thickness in the longitudinal direction. The bubble nucleation for 1-fm time obtained from the nucleation rate given in Eqs. (9) and (10) leads to about three to five bubbles in this region. (The approach followed in Ref. [30] gives the nucleation rate of about 10^{-4} fm^{-4} in the relevant temperature range, leading to negligible nucleation of bubbles).

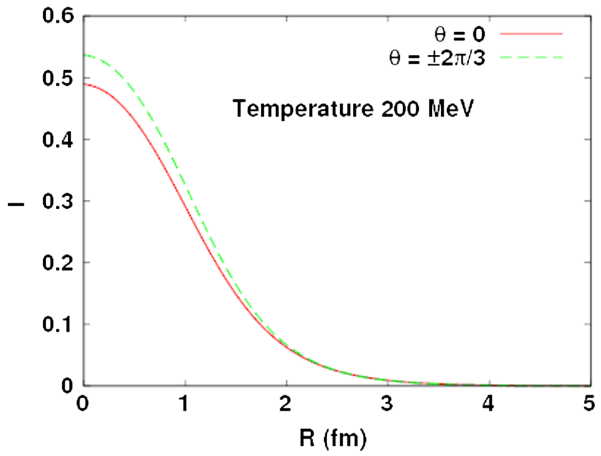

FIG. 2 (color online). Critical bubble profiles for the different Z(3) vacua for $b_1 = 0.005$.

One may expect that the nucleation rate of the two metastable Z(3) vacua will be smaller than that of the true Z(3) vacuum due to larger action S_3 of the metastable vacuum leading to exponential suppression. However, here we see an interesting interplay between the exponential factor $e^{-S_3(T)/T}$ [Eq. (9)] and the prefactor A as given in Eq. (10). If $S_3(T)$ is much larger than T then the nucleation rate is dominated by the exponential factor confirming the above expectation. Thus, the nucleation rate of the metastable vacuum bubble is much smaller than the true vacuum bubble when the temperature is closer to T_c. The nucleation rate of the true vacuum bubble and metastable vacuum bubble at a temperature near T_c (at $T = 185$ MeV) is of the order of $\sim 1.3 \times 10^{-5}$ fm^{-4} and $\sim 3.4 \times 10^{-7}$ fm^{-4}, respectively. As we increase the temperature from $T_c = 182$ MeV, the nucleation rate of the metastable vacuum bubble increases and becomes almost equal to that of the true vacuum bubble at $T \simeq 200$ MeV (both rates being $\sim 2.4 \times 10^{-2}$ fm^{-4}). This happens because at these temperatures $S_3 \simeq T$ so that the decrease of the exponential term for a larger S_3 (corresponding to the metastable vacuum) is not very significant. However, the preexponential factor A in Eq. (10) increases with S_3, and this increase of the prefactor term starts dominating the exponential factor in the nucleation rate equation for $T \geq 200$ MeV. For higher temperatures, the nucleation rate for metastable vacuum bubbles becomes larger than the true vacuum bubbles. The nucleation rates of metastable and true vacuum bubbles at temperature 215 MeV are the order of $\sim 1.5 \times 10^{-2}$ fm^{-4} and 7.7×10^{-3} fm^{-4}, respectively. At higher temperatures though, the nucleation rate for both bubbles decreases, but the metastable bubble nucleation rate remains larger. This result is very interesting as it shows that at suitable temperatures the metastable Z(3) vacua will have a larger nucleation rate than the true Z(3) vacuum. Further, these metastable vacuum bubbles are also of larger size than the bubble of true vacuum. Thus, one may expect a larger fraction of the QGP region to end up in the metastable Z(3) vacuum regions after the phase transition, which may have interesting implications. For example, we will see below that the metastable vacuum bubble walls have a much higher concentration of energy density than the true vacuum bubble walls. We will use $T = 200$ MeV for the bubble nucleation, as the nucleation

rates are the same for both the true vacuum and metastable vacuum bubbles.

V. NUMERICAL TECHNIQUES

In this work, we carry out a $2+1$ dimensional field theoretic simulation of the formation and evolution of QGP phase bubbles representing the central rapidity region of QGP in RHICE. Bubbles are nucleated randomly in the confining background. We calculate the bubble profiles in $3+1$ dimensions and use these profiles for the evolution in $2+1$ dimensions. As explained above, this represents transverse evolution of these bubbles by field equations and their longitudinal evolution is simply given by the Bjorken longitudinal expansion [31]. We nucleate bubbles at the temperature 200 MeV at which the metastable and true vacuum bubbles have the nucleation rates of the same order $\simeq 0.024\ \mathrm{fm}^{-4}$ so that the number of metastable and true vacuum bubbles seeded remains almost equal. Initially the the field $l(\vec{x})$ is zero everywhere, and the bubbles of the QGP phase are nucleated over the whole lattice with random choice of their location. (Again, recall that we are using the shifted field here with $b_1 \neq 0$). The bubbles are nucleated with the condition that one bubble should not overlap with the other. We implement this condition by checking whether or not the region where the bubble is going to be nucleated lies in the false vacuum. If in the region a bubble has seeded already, the next bubbles will be seeded at some other random position with the same conditions. (These techniques for the formation and evolution of bubbles in a first order transition are the same as those used in Ref. [32].)

We take the initial temperature of the system to be zero (representing the initial confining system), and it is taken to increases linearly with time up to $T = 400$ MeV at (proper) time $\tau = \tau_0 = 1$ fm. The bubble nucleation is possible only in the range of temperatures where the transition is of first order. The barrier in between false vacuum and true vacuum as well as false vacuum and metastable vacua of Eq. (5) exists only for the temperature $T = 182$ MeV to $T \simeq 225$ MeV for our chosen value of $b_1 = 0.005$. The nucleation of bubbles is possible only during the time when the temperature linearly increases from $T = T_c = 182$ MeV to $T \simeq 225$ MeV. In order to have a reasonable range of temperatures for bubble nucleation and evolution, we nucleate bubbles at $T = 200$ MeV. Note that the bubbles should also be nucleated at higher temperatures, say near $T = 225$ MeV. These will be smaller in size. Along with such bubbles there will also be subcritical bubbles that will shrink fast and disappear due to the surface energy domination. Such bubbles should be incorporated to account for fluctuations [32], but we will ignore these here.

In RHICE, the QGP bubbles are nucleated in the hadronic phase during the time span when the temperature changes from the transition temperature to the maximum temperature $T_0 = 400$ MeV in the preequilibrium stage; hence, this should lead to the presence of metastable and true vacuum bubbles of different sizes at a given time. These bubbles expand in hadronic background with time, and ultimately the whole system gets converted to the QGP phase. We choose to seed the bubbles at a fixed nucleation temperature because the QGP bubbles being nucleated in hadronic background have zero velocity initially and remain almost static during the remaining preequilibrium time $\simeq 0.5$ fm when the temperature increases from $T = T_c = 182$ MeV to $T = T_0 = 400$ MeV. The growth of bubbles nucleated at different time and the increase in their velocity until the temperature reaches 400 from the nucleation temperature are negligible in this short time span. Therefore, for simplicity our choice to seed bubbles at a fixed temperature is a reasonable approximation. We choose $T = 200$ MeV as at this temperature the true vacuum and the metastable vacuum bubbles have almost equal nucleation rates and both kinds of bubbles are possible with equal probability. This provides us a better opportunity to study the dynamics of metastable vacuum bubbles together with that of true vacuum bubbles, and its effect on the evolution of true vacuum bubbles.

After nucleation, the bubbles are evolved by the time dependent equation of motion in Minkowski space [33]:

$$\frac{\partial^2 l_j}{\partial \tau^2} + \frac{1}{\tau}\frac{\partial l_j}{\partial \tau} - \frac{\partial^2 l_j}{\partial x^2} - \frac{\partial^2 l_j}{\partial y^2} = -\frac{g^2}{2NT^2}\frac{\partial V(l)}{\partial l_j}; \quad j = 1, 2 \tag{11}$$

with $\frac{\partial l_j}{\partial \tau} = 0$ at $\tau = 0$ and $l = l_1 + i l_2$.

We take a 2000×2000 lattice with a physical size of 16 fm $\times$ 16 fm (as appropriate for an Au-Au collision in RHICE). We take this lattice as the transverse plane of the QGP formed in a central collision and consider the longitudinal extension of 1 fm in the midrapidity region. The evolution of metastable and true vacuum bubbles with different Z(3) vacuum inside gives rise to the domain wall and string networks. The domain walls form when the two bubbles of different Z(3) vacua coalesce with each other. The intersection of three domain walls forms a string. In our simulation, these objects are formed in the transverse plane. Hence, the domain walls appear as curves while the cross section of three-dimensional strings appear as vortices.

In the relativistic heavy-ion collision, the thermalization time for an Au-Au collision at 200 MeV is expected to be $\tau \leq 1$-fm time. As mentioned above, we model the system in our simulation such that there is a linear increase in temperature in the preequilibrium stage; it starts from $T = 0$ and reaches a maximum value of $T = 400$ within time $\tau = 0$ to $\tau = \tau_0 = 1$. After that, it decreases according to Bjorken's scaling due to the continued expansion in longitudinal direction [31]

$$T(\tau) = T(\tau_0)\left(\frac{\tau_0}{\tau}\right)^{1/3}. \tag{12}$$

In our numerical simulation, we evolve the field using the periodic, fixed, and free boundary conditions for the square lattice. We present our results for the free boundary condition case where the field (waves) crossing the boundary during evolution go out permanently. This condition minimizes effects due to boundary points in the evolution of field (for example, field reflection from boundary points in fixed boundary condition and mirror reflection as in periodic boundary condition). We use additional dissipation in a thin strip of ten points near the boundary to reduce the (minor) boundary effects in the use of free boundary conditions. To represent the situation of heavy-ion collision experiments, we nucleate bubbles within a circular region of 8-fm radius on the lattice of physical size 16 fm $\times$ 16 fm. With $\Delta x = 0.008$ fm, we use $\Delta t = \Delta x/\sqrt{2}$ and $\Delta t = 0.9\Delta x/\sqrt{2}$ to satisfy the Courant stability criteria. The stability and accuracy of the simulation is checked using the conservation of energy during simulation. The total energy fluctuations remain a few percent without any net increase or decrease of total energy in the absence of dissipative $\dot{l}$ term in Eq. (11) as well as any other dissipation for periodic and fixed boundary conditions.

VI. RESULTS OF THE SIMULATION

The general picture of the phase transition remains similar to the case of $b_1 = 0$ discussed in Ref. [1], but there are important differences. We show in Fig. 3 the various stages of the formation and evolution of different Z(3) bubbles and the subsequent formation and evolution of Z(3) walls and strings. In order for one to compare the $b_1 = 0$ case with the case discussed in Ref. [1], we present in Fig. 3 the case of five bubbles in a 16 fm $\times$ 16 fm region, similar to the case discussed in Ref. [1]. Figure 3(a) shows the initial plot of $l(x)$ showing the nucleation of five bubbles at $\tau = 0.5$ fm. Figure 3(b) shows the plot of $l(x)$ at $\tau = 1.5$ fm showing the expansion of bubbles. Figure 3(c) shows the plot of the phase of $l(x)$ at the initial stage, and Fig. 3(d) shows the phase plot at $\tau = 3.2$ fm showing clearly the formation of domain walls and a QGP string near ($x = 8$ fm, $y = 9$ fm). The important difference in the dynamics of true vacuum bubbles and the metastable vacuum bubbles can be seen in the surface plots of energy density (in GeV/fm^3) at $\tau = 0.75$ fm [Fig. 3(e)] and at $\tau = 2.6$ fm [Fig. 3(f)]. Note that in all the figures we plot energy density in GeV/fm^3 as we are considering the central rapidity region with thickness of about 1 fm. With similar energy densities to begin with, by the time $\tau = 2.6$ fm, the energy density at the walls of the bubbles of true vacuum is much smaller than the energy density of the walls for the false vacuum bubbles.

A. Variance of energy density

The general evolution of bubble coalescence and the formation of walls and strings are similar to those shown in Ref. [1] for the $b_1 = 0$ case, and we do not show those here. As we are discussing the case of a relatively small value of b_1 here, we do not expect dramatic effects arising from explicit symmetry breaking (e.g., from the different mechanism of production of topological objects as demonstrated in Ref. [26]). However, it is still important to see if there are any qualitative differences between the $b_1 = 0$ case and the $b_1 \neq 0$ case. We find an interesting difference in the plot of the standard deviation of energy density between the two cases. We calculated the standard deviation σ of the energy density at each time stage to study how energy fluctuations change during the evolution. In Fig. 4

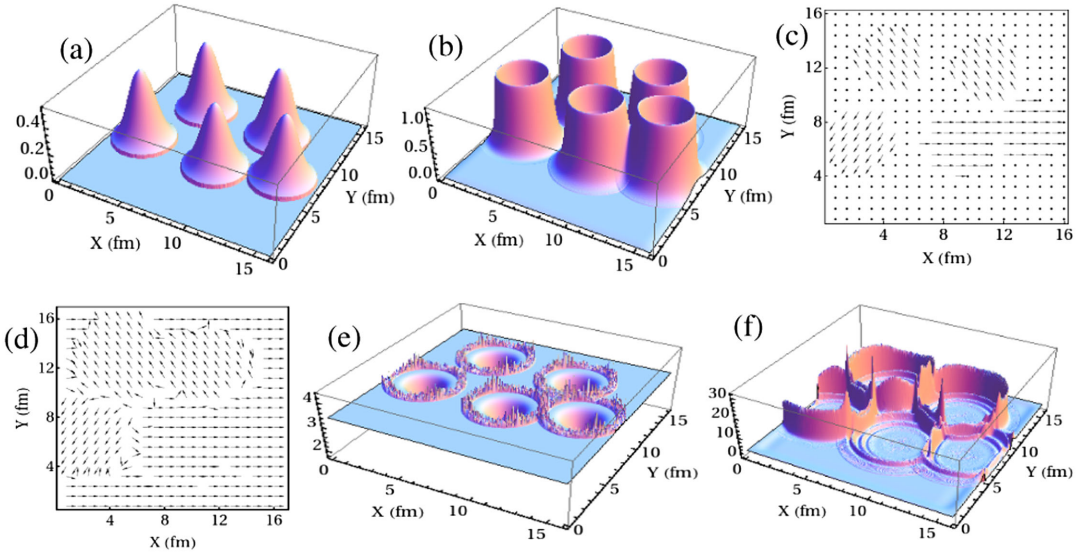

FIG. 3 (color online). (a) and (b) show plots of profiles of l at $\tau = 0.5$ and 1.5 fm, respectively, showing expansion of bubbles. (c) and (d) show the plots of the phase of l at $\tau = 0.5$ and 3.2 fm. (e) and (f) show the surface plots of energy density (in GeV/fm^3) at $\tau = 0.75$ and 2.6 fm showing very different energetics of the walls of the true vacuum bubbles and the metastable vacuum bubbles.

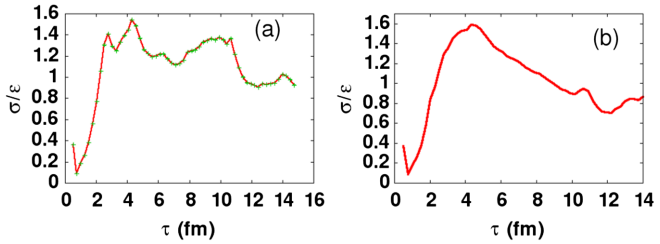

FIG. 4 (color online). (a) and (b) show plots of the ratio of standard deviation of energy density σ and the average energy density ε as a function of proper time for the $b_1 = 0.005$ case and the $b_1 = 0$ case, respectively. Error bars in (a) are very small, about three orders of magnitude smaller than the values of σ/ε. The same holds for all the plots [for (b) and in the figures below]; hence, we do not show error bars for other plots.

we show the plot of σ/ε as a function of proper time. Here ε is the average value of energy density at that time stage. The energy density ε decreases due to longitudinal expansion; hence, we plot this ratio to get an idea of the relative importance of energy density fluctuations. For comparison, we reproduce such a plot from Ref. [1] for the $b_1 = 0$ case in Fig. 4(b). We note that fluctuations have an overall tendency to decrease in Fig. 4(b) while there seems no such decrease in Fig. 4(a) for the case with quark effects. Note also the presence of a peak for small times near $\tau \simeq 3$ fm in the $b_1 > 0$ case. There is no such sharp peak for the $b_1 = 0$ case. The remaining features of the plot can be interpreted as follows. The initial rapid drop in σ/ε is due to a large increase in ε during the heating stage up to $\tau = 1$ fm followed by a rise due to increased energy density fluctuations during the stage when the bubbles coalesce and the bubble walls decay, as expected. The peak in the plot near $\tau = 10$ fm when T drops below T_c should correspond to the decay of domain walls and may provide a signal for the formation and subsequent decay of such objects in RHICE. We have plotted error bars in Fig. 4(a); these are very small, about three orders of magnitude smaller than the values of σ/ε. The same holds for all the plots [for Fig. 4(b) and in the figures below]; hence, we do not show error bars for other plots.

The small peak at short times for the $b_1 > 0$ case seems to arise from the difference between the collisions of metastable vacuum bubbles and true vacuum bubbles and hence seems of qualitative importance. We have checked for various situations, different number of bubbles, etc., and this peak is always present. Figure 5 shows different cases for a number of bubbles ranging from four to ten, and we see the presence of this peak in all these cases. We mention here that a significantly large peak for the ten-bubble case in Fig. 5(f) (near $\tau = 10$ fm) is due to the collapse of a closed wall at that time (as we will see later in the Sec. VI C below). The closed wall is more likely to form with a larger number of bubbles. As the wall collapses, it concentrates a large amount of energy in a localized region and leads to a large fluctuation in energy density.

We note that the error bars in Fig. 4(a) (which are very small) represent uncertainty in the value of σ/ϵ for a given event (meaning the given realization of the bubble configurations) at specific stages. Even though this is small, it is important to know how much uncertainty is there due to different random realizations of the same event (meaning the same number of bubbles, which will presumably correspond to considering the same types of events with centrality, energy, etc.). For this purpose, we have carried out simulations of different random realizations of the five-bubble case

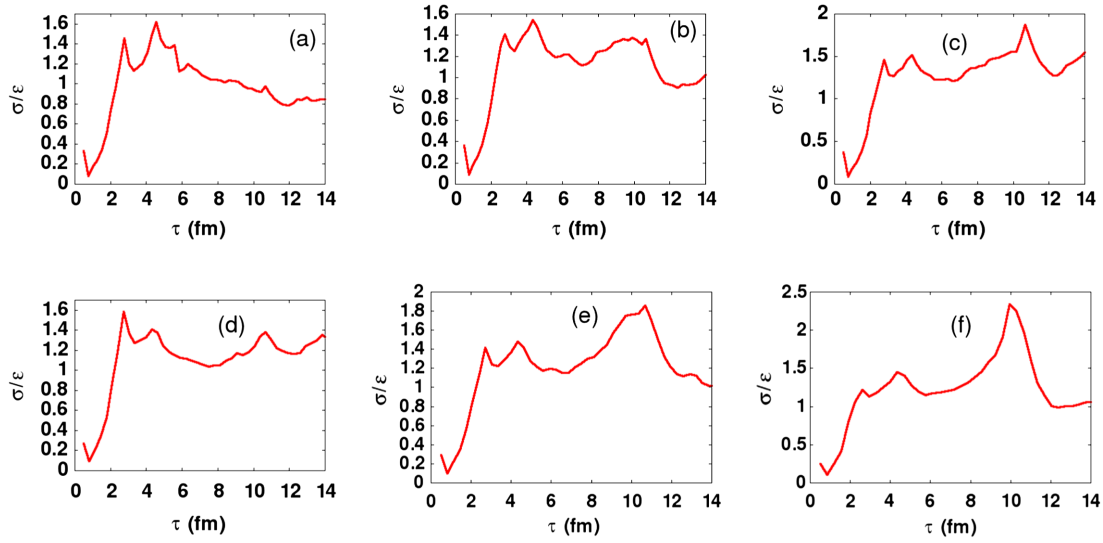

FIG. 5 (color online). Plots of the ratio σ/ε as a function of proper time for the $b_1 = 0.005$ case for a different number of bubbles. (a)–(f) show curves for number of bubbles = 4, 5, 5 (different realization), 7, 8, and 10, respectively. Note the presence of a small peak for short times in all these cases. Also note that there is no overall decrease for long times as was seen in Fig. 4(b) for the $b_1 = 0$ case.

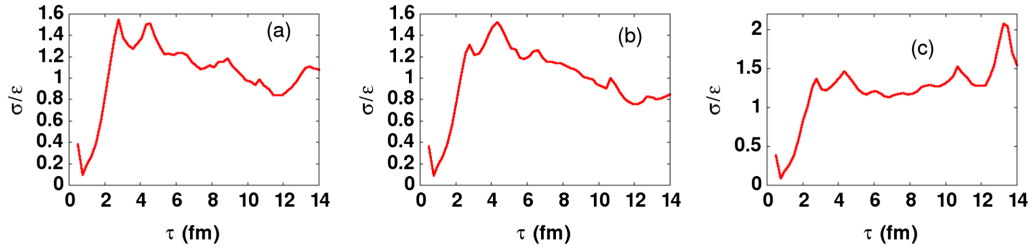

FIG. 6 (color online). Plots of the ratio σ/ε for different realizations of the five-bubble case, as in Figs. 5(b) and 5(c). These different realizations show how this plot of σ/ε can vary from one event to another, even if the number of bubbles remains the same.

[such as those shown in Figs. 5(b) and 5(c)]. These different realizations are shown in Fig. 6. These different realizations of five-bubble configurations and the resulting differences in plots of σ/ϵ between these plots represent event-by-event fluctuations in these plots. We note that these variations are large from one event to another (such as a peak at the last stages), though all these plots appear to consistently show more fluctuations [compared to Fig. 4(b)].

B. Wall velocity

An important difference we note is in the wall velocity. We have estimated wall velocities for the domain walls separating the two degenerate metastable Z(3) vacua, and the metastable and the true vacuum. We find that the typical velocity of the domain walls separating the two (degenerate) metastable vacua is 0.7–0.8, similar to that obtained in Ref. [1] for the $b_1 = 0$ case. This is certainly expected. However, the velocity of the domain wall separating the true vacuum and the metastable vacuum is found to be much larger in many cases, close to 1. Very accurate wall velocity estimates are not possible due to uncertainties in identifying wall location (with dynamically evolving wall profile). We show in Figs. 7 and 8 two different cases of five-bubble nucleations (with different locations and phases inside the bubbles). Contour plots of energy density are shown in Figs. 7(a) and 7(b) at $\tau = 7.2$ and 7.8 fm (the temperature at these stages is 208 and 201 MeV, respectively). The portion of the domain wall near $x = 14$ fm, $y = 12$ fm in Fig. 7(a) is seen to move towards the left in Fig. 7(b) with $v \simeq 1$. This is confirmed by the profile plot of $l_0 - l$ in Figs. 7(c) and 7(d) at the same stages, $\tau = 7.2$ and 7.8 fm, respectively.

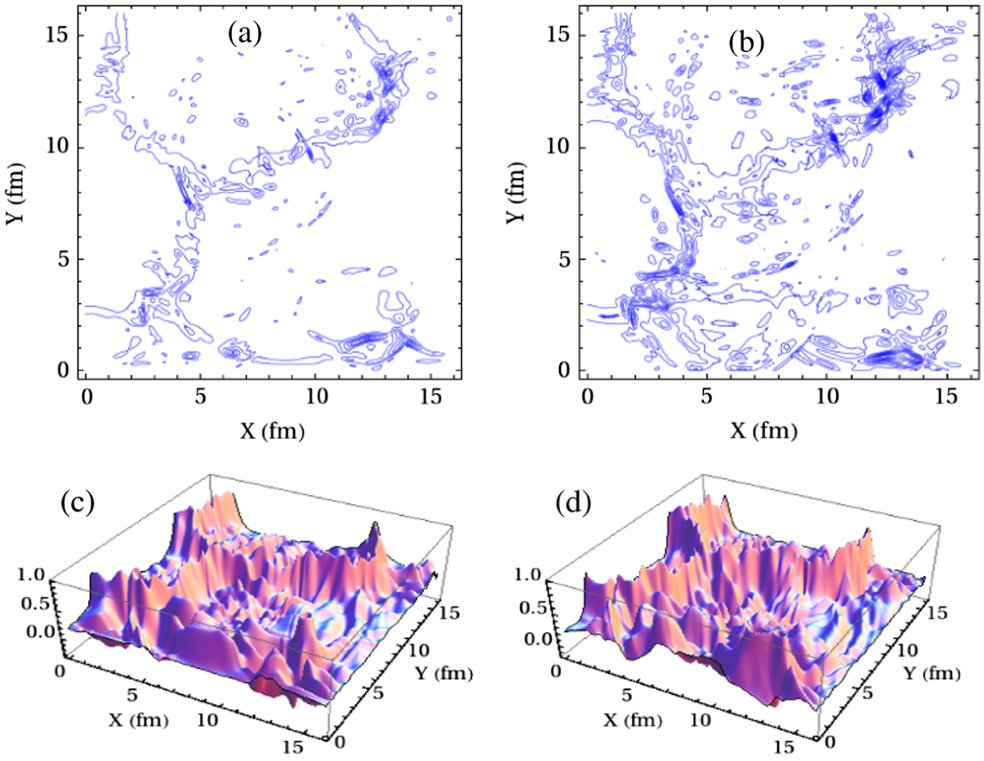

FIG. 7 (color online). Contour plot of energy density at (a) $\tau = 7.2$ fm and (b) at $\tau = 7.8$ fm. Wall portion near $x = 14$ fm, $y = 12$ fm in (a) is seen to move towards the left in (b) with large velocity. (c) and (d) show the profile plots of $l_0 - l$ at these stages confirming the motion of the domain wall.

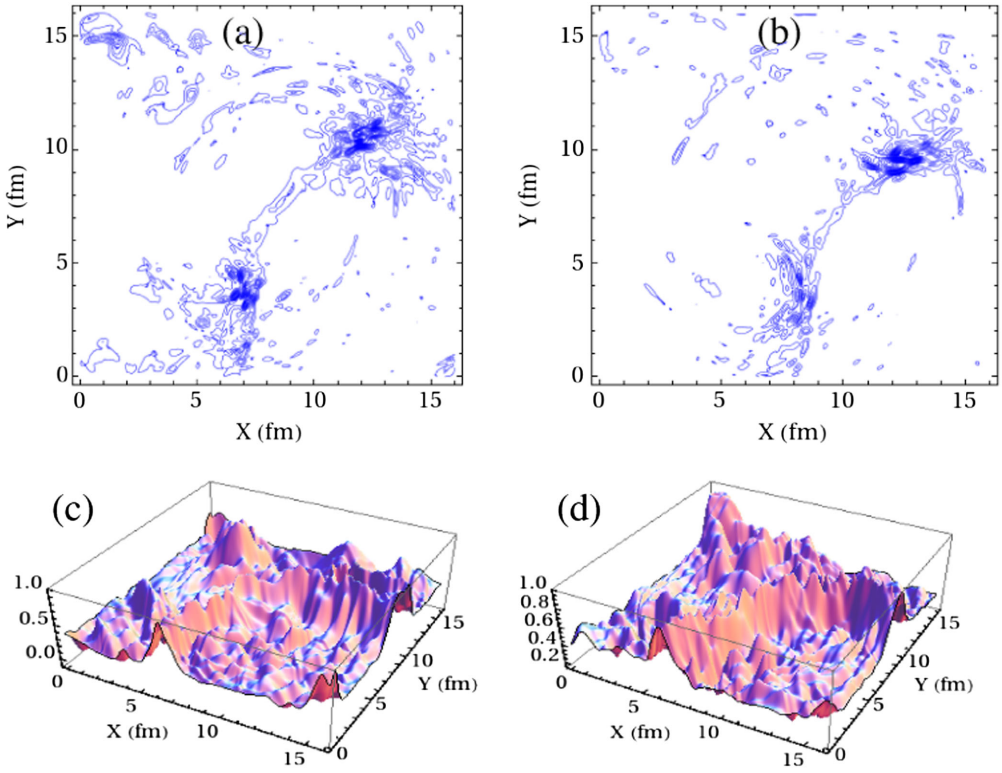

FIG. 8 (color online). A different realization of five-bubble nucleation. Contour plot of energy density at (a) $\tau = 9.6$ fm and (b) at $\tau = 10.9$ fm. Wall portion near $x = 9$ fm, $y = 8$ fm in (a) is seen to move towards the lower right in (b) with large velocity. (c) and (d) show the profile plots of $l_0 - l$ at these stages confirming the motion of the domain wall.

Figure 8 shows another case of five-bubble nucleation. Figures 8(a) and 8(b) show the contour plots of energy density at $\tau = 9.6$ and 10.9 fm. The temperature at these stages is $T = 188$ and 180 MeV (note, this is slightly below T_c). The location of the wall in Fig. 8(a) is near $x = 9$ fm, $y = 8$ fm, and this is seen to move towards the lower right corner. This wall motion is confirmed by the profile plots of $l_0 - l$ in Figs. 8(c) and 8(d).

We again emphasize that it is very difficult to give an error estimate for the bubble wall velocity primarily due to its fluctuating width and shape. An estimate of the uncertainty in velocity is already mentioned above with velocity being 0.7–0.8. Similar uncertainty applies to the case of velocity being close to 1 also. As can be seen from the contour plots and from the surface plots, the wall represents a broad profile and highly fluctuating shape. Even the profile is different at different points. Note that these walls cannot be traced by following a zero of the field (as in the case of the real scalar field). The location of the wall here (where l remains nonzero across the wall) cannot be determined accurately.

C. Rapid collapse and reexpansion

Perhaps the most dramatic difference between the present case with $b_1 \neq 0$ and the previous case [1] of $b_1 = 0$ is seen in Figs. 9 and 10. This shows the case of nucleation of ten bubbles in a region of 22 fm $\times$ 22 fm. Though both of these numbers are somewhat large for RHICE, at least the size may not be too unrealistic for later stages of plasma evolution. Figure 9 shows a time sequence of the contour plot of energy density at $\tau = 6.44$, 8.20, 9.94, 11.34, 12.74, and 14.5 fm. The temperature at these stage is $T = 215.0$, 198.4, 186.0, 178.0, 171.2, and 164.1 MeV, respectively. Note that T is below T_c in Fig. 9(d), and remains so for Figs. 9(e) and 9(f). A closed domain wall is seen $y = 5$–11 fm. The collapse velocity again is seen to be close to $v \simeq 1$. Interesting dynamics is seen for later plots when an expanding front is seen from the point of collapse. It rapidly expands again with $v \simeq 1$ all the way until the last stages in Fig. 9(f). The presence of such an energetic expanding front is confirmed by the surface plots of energy density at the same stages as shown in Fig. 10. Due to the very large velocity and sharp profile of the expanding front, it may well represent a shock front in the plasma. We emphasize that the reexpansion shown here represents an expanding energy front. This has nothing to do with bubble collapse or expansion. The collapsing structure here [in Figs. 9(a)–9(c)] represents a collapsing closed Z(3) domain wall which itself was formed by the coalescence of several bubbles. This closed Z(3) domain wall completely collapses and disappears by Fig. 9(c). As there is a huge energy concentration at the point of collapse, this leads to an expanding energy front [Figs. 9(d)–9(f)] which is also circular, but it is not a wall structure.

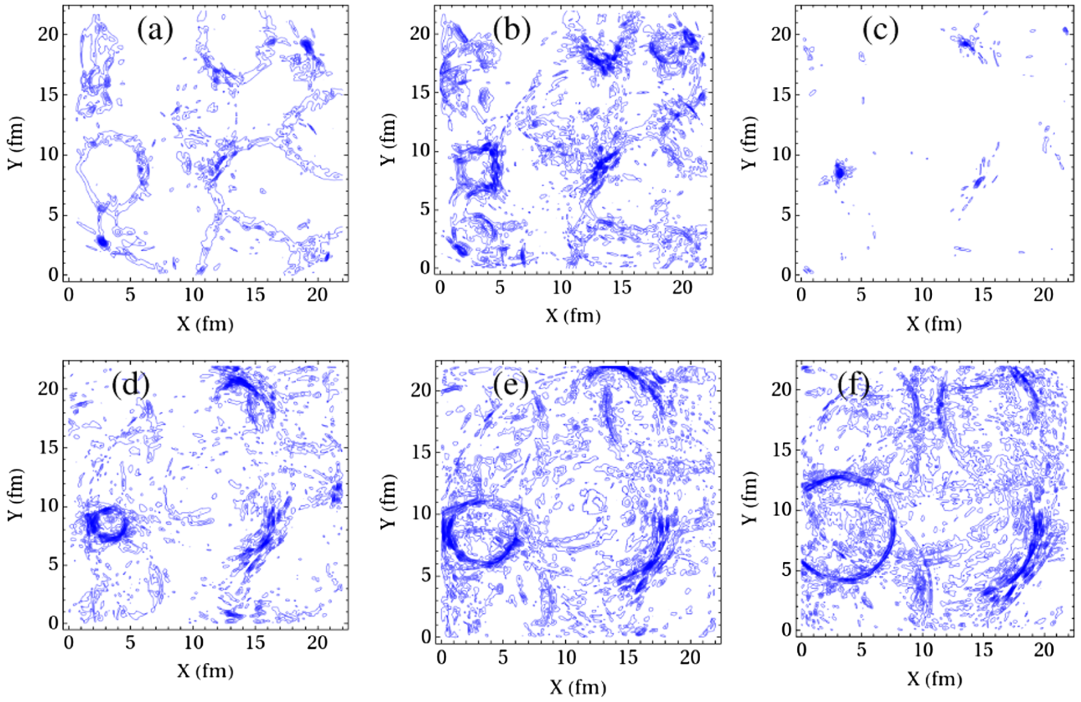

FIG. 9 (color online). A case of ten bubbles in a 22 fm $\times$ 22 fm region. This figure shows a time sequence of the contour plot of energy density at $\tau = 6.44$, 8.20, 9.94, 11.34, 12.74, and 14.5 fm. The temperatures at these stages are $T = 215.0$, 198.4, 186.0, 178.0, 171.2, and 164.1 MeV, respectively. Contour plots show rapid collapse of a domain wall (towards the lower left) and subsequent rapid expansion of a circular front.

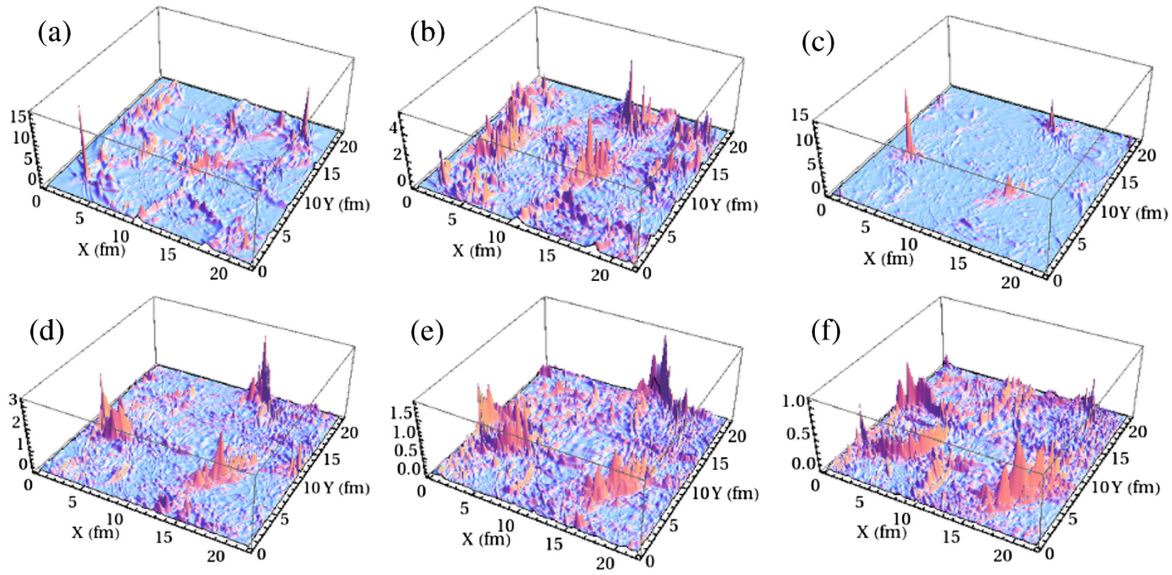

FIG. 10 (color online). Surface plots of energy density for various stages shown in Fig. 10.

VII. POSSIBLE EXPERIMENTAL SIGNATURES OF Z(3) WALLS AND STRINGS WITH EXPLICIT SYMMETRY BREAKING

The Z(3) wall network and associated strings exist only during the QGP phase, melting away when the temperature drops below T_c. However, they may leave their signatures in the distribution of final particles due to a large concentration of energy density in the extended regions, and due to nontrivial scatterings of quarks and antiquarks with these objects. The extended regions of high energy density resulting from the domain walls and strings are clearly seen in our simulations, and some extended structures/hot spots also survive after the temperature drops below the

transition temperature T_c. This is just as was seen in the $b_1 = 0$ case in Ref. [1]. We again mention that even the hot spot resulting from the collapse of closed domain walls in our simulations will be stretched in the longitudinal direction into an extended linear structure (resulting from the collapse of a cylindrical wall). These may be observable in the analysis of particle multiplicities. This is important especially in respect to the ridge phenomenon seen in RHIC [34]. In view of lasting extended energy density fluctuations from Z(3) walls, it is of interest to check if these structures can account for the ridge phenomenon.

Our results show an interesting pattern of the evolution of the fluctuations in the energy density: these fluctuations do not decrease with time, which was the case for the $b_1 = 0$ case studied in Ref. [1]. Especially important may be the presence of a small additional peak of short times for the $b_1 > 0$ case. Fluctuations near the transition stage may leave direct imprints on particle distributions. However, dileptons or direct photons should be sensitive to these fluctuations, and these may give a time history of evolution of such energy density fluctuations during the early stages. In such a case, the existence of a small peak for the $b_1 > 0$ case may be observable.

A dramatic difference between the cases of $b_1 = 0$ and $b_1 \neq 0$ is seen in Figs. 9 and 10. Collapse of a closed wall is expected and was seen for the $b_1 = 0$ case also, though the wall speed here is much higher, close to 1. In general we have seen here that walls separating true vacuum from metastable vacuum have speeds much higher than those seen for the case of $b_1 = 0$. What is qualitatively new in the present case is a rapidly expanding circular front after the collapse of the wall. This front continues its speed and shape even when temperature drops below T_c. The possibility of such expanding circular (cylindrical with longitudinal expansion) energetic fronts should have important implications on particle momenta, especially on various flow coefficients.

Another important difference due to $b_1 > 0$ is expected in investigating the interactions of quarks and antiquarks with domain walls. Earlier we argued [1] that collapsing Z(3) walls would lead to a concentration of quarks (due to small nonzero chemical potential in RHICE) in small regions [3]. This will lead to an enhancement of baryons, especially at high P_T [20] due to P_T enhancement of quarks/antiquarks as they undergo repeated reflections from a collapsing wall. (There is also a possibility of spontaneous CP violation in the scattering of quarks and antiquarks from Z(3) walls, see Ref. [35].) However, with $b_1 > 0$ there may also be a possibility that a Z(3) wall may actually expand (the one enclosing the true vacuum and with sufficiently large size). In that case it will have the opposite effect, and the baryon number will be more diffused. Even the enhancement of P_T may happen for some domain walls (those which enclose metastable vacuum) while the expanding closed walls (enclosing the true vacuum) should lead to the redshift of the momenta for the enclosed quarks. All these issues need to be explored with more elaborate simulations. In this context, the difference in the wall velocity between different types of Z(3) walls is of importance. While studying the effects of quark reflections from these walls and the associated modification of P_T spectrum, wall velocity is of crucial importance, and the presence of different types of collapsing Z(3) walls may lead to bunches of hadrons with different patterns of modified P_T spectra.

VIII. CONCLUSIONS

We studied the effects of explicit symmetry breaking arising from quark effects on the formation and evolution of Z(3) interfaces and associated strings. Explicit symmetry breaking makes Z(3) vacua nondegenerate with two vacua $l = z, z^2$ remaining degenerate with each other but having higher energy than the true $l = 1$ vacuum. Thus, $l = z, z^2$ vacua become metastable. We used an effective potential for the Polyakov loop expectation value $l(x)$ from Refs. [9,10] with incorporation of explicit symmetry breaking in terms of a linear term in l, and we studied the dynamics of the C-D phase transition in the temperature/time range when the first order transition of this model proceeds via bubble nucleation. This allows for only relatively small explicit symmetry breaking (characterized by the strength b_1 of the linear term in l). We again emphasize that though our study is in the context of a first order transition, certain aspects of our results are expected to be valid even when the transition is a crossover. This is because our focus is primarily on the formation of topological objects whose formation (via Kibble mechanism) only depends on the formation of a domain structure and not crucially on the dynamics of the phase transition. Though our statements about the energetics of bubble walls, etc., clearly apply only for a first order transition. These results will not be relevant for ultrarelativistic heavy-ion collisions which relate to rather small values of chemical potentials where the transition is expected to be a crossover. Our results with detailed dynamics of first order transition will be relevant for lower energy collisions which explore relatively high chemical potential regime of the QCD phase diagram. We also point out that the relevance of quarks for phase transition is not only for discussing metastability of different Z(3) vacua. We focused on confinement-deconfinement transition. However, for chiral phase transition the effects of quarks will also relate to the universal scaling behavior in the chiral limit, which may still be relevant for physical light quark masses. These issues can be studied by carrying out simulations like in the present paper for chiral models with Polyakov loop coupling.

An important result we discussed in this paper relates to the expected relative importance of the metastable Z(3) vacua. Due to the higher energy of these vacua, one would expect that bubbles with these vacua should form with relatively lower probability (even with the small values of b_1 we used). However, we find interesting results due to nontrivial interplay of the preexponential factor and the exponential

term in the nucleation rate for the bubbles. While the exponential term leads to a decrease in the rate for metastable vacua due to larger action, the preexponential factor leads to an increase in the rate for larger action. For a suitable range of temperatures, which for our choice of parameter values lies between $T = 200$ MeV to $T = 225$ MeV, the metastable vacuum bubbles have the same or larger nucleation rate compared to the true vacuum bubbles. As the metastable vacuum bubbles also have larger sizes, it means that a larger fraction of QGP phase may get converted to the metastable Z(3) vacua than to the true Z(3) vacuum. The dynamics of these domains being so different, its effects on the evolution of plasma and various signals may be important.

ACKNOWLEDGMENTS

We are very grateful to Sanatan Digal, Anjishnu Sarkar, Ananta P. Mishra, P. S. Saumia, and Abhishek Atreya for very useful comments and suggestions. U. S. G, A. M. S., and V. K. T. acknowledge the support of the Department of Atomic Energy-Board of Research in Nuclear Sciences (DAE-BRNS), India, under the research Grant No. 2008/37/13/BRNS. U. S. G. and V. K. T. acknowledge support of the computing facility developed by the Nuclear-Particle Physics Group of the Physics Department, Allahabad University under the Center of Advanced Studies (CAS) funding of UGC, India.

[1] U. S. Gupta, R. K. Mohapatra, A. M. Srivastava, and V. K. Tiwari, Phys. Rev. D **82**, 074020 (2010).
[2] B. Layek, A. P. Mishra, and A. M. Srivastava, Phys. Rev. D **71**, 074015 (2005).
[3] B. Layek, A. P. Mishra, A. M. Srivastava, and V. K. Tiwari, Phys. Rev. D **73**, 103514 (2006).
[4] L. D. McLerran and B. Svetitsky, Phys. Rev. D **24**, 450 (1981); B. Svetitsky, Phys. Rep. **132**, 1 (1986).
[5] T. Bhattacharya, A. Gocksch, C. K. Altes, and R. D. Pisarski, Nucl. Phys. **B383**, 497 (1992); J. Boorstein and D. Kutasov, Phys. Rev. D **51**, 7111 (1995).
[6] A. V. Smilga, Ann. Phys. (N.Y.) **234**, 1 (1994).
[7] V. M. Belyaev, I. I. Kogan, G. W. Semenoff, and N. Weiss, Phys. Lett. B **277**, 331 (1992).
[8] C. P. Korthals-Altes, arXiv:hep-th/9402028.
[9] R. D. Pisarski, Phys. Rev. D **62**, 111501(R) (2000); arXiv: hep-ph/0101168.
[10] A. Dumitru and R. D. Pisarski, Phys. Lett. B **504**, 282 (2001); Phys. Rev. D **66**, 096003 (2002); Nucl. Phys. **A698**, 444 (2002).
[11] M. Deka, S. Digal, and A. P. Mishra, Phys. Rev. D **85**, 114505 (2012).
[12] A. Dumitru, D. Roder, and J. Ruppert, Phys. Rev. D **70**, 074001 (2004).
[13] T. Banks and A. Ukawa, Nucl. Phys. **B225**, 145 (1983).
[14] F. Green and F. Karsch, Nucl. Phys. **B238**, 297 (1984).
[15] P. N. Meisinger and M. C. Ogilvie, Phys. Rev. D **52**, 3024 (1995).
[16] S. Digal, E. Laermann, and H. Satz, Nucl. Phys. **A702**, 159 (2002); F. Karsch, E. Laermann, A. Peikert, C. Schmidt, and S. Stickan, Nucl. Phys. B, Proc. Suppl. **94**, 411 (2001).
[17] J. Ignatius, K. Kajantie, and K. Rummukainen, Phys. Rev. Lett. **68**, 737 (1992); V. Dixit and M. C. Ogilvie, Phys. Lett. B **269**, 353 (1991).
[18] T. W. B. Kibble, J. Phys. A **9**, 1387 (1976); Phys. Rep. **67**, 183 (1980).
[19] W. H. Zurek, Phys. Rep. **276**, 177 (1996).
[20] A. P. Mishra, A. M. Srivastava, and V. K. Tiwari, Indian J. Phys. **85**, 1161 (2011).
[21] A. Bazavov, B. A. Berg, and A. Dumitru, Phys. Rev. D **78**, 034024 (2008).
[22] K. Fukushima, Phys. Lett. B **591**, 277 (2004); S. Rosner, C. Ratti, and W. Weise, Phys. Rev. D **75**, 034007 (2007); D. Diakonov and M. Oswald, Phys. Rev. D **70**, 105016 (2004).
[23] O. Scavenius, A. Dumitru, and J. T. Lenaghan, Phys. Rev. C **66**, 034903 (2002).
[24] G. Boyd, J. Engels, F. Karsch, E. Laermann, C. Legeland, M. Lutgemeier, and B. Petersson, Nucl. Phys. **B469**, 419 (1996); M. Okamoto *et al.*, Phys. Rev. D **60**, 094510 (1999).
[25] S. Chang, C. Hagmann, and P. Sikivie, Phys. Rev. D **59**, 023505 (1999); M. C. Huang and P. Sikivie, Phys. Rev. D **32**, 1560 (1985).
[26] S. Digal and A. M. Srivastava, Phys. Rev. Lett. **76**, 583 (1996); S. Digal, S. Sengupta, and A. M. Srivastava, Phys. Rev. D **55**, 3824 (1997).
[27] I. Y. Kobzarev, L. B. Okun, and M. B. Voloshin, Yad. Fiz. **20**, 1229 (1974) [Sov. J. Nucl. Phys. **20**, 644 (1975)]; S. Coleman, Phys. Rev. D **15**, 2929 (1977).
[28] A. D. Linde, Nucl. Phys. **B216**, 421 (1983).
[29] J. S. Langer, Ann. Phys. (N.Y.) **54**, 258 (1969); J. S. Langer and L. A. Turski, Phys. Rev. A **8**, 3230 (1973); L. A. Turski and J. S. Langer, Phys. Rev. A **22**, 2189 (1980).
[30] L. P. Csernai and J. I. Kapusta, Phys. Rev. D **46**, 1379 (1992); J. I. Kapusta, A. P. Vischer, and R. Venugopalan, Phys. Rev. C **51**, 901 (1995).
[31] J. D. Bjorken, Phys. Rev. D **27**, 140 (1983).
[32] A. M. Srivastava, Phys. Rev. D **45**, R3304 (1992); **46**, 1353 (1992); S. Chakravarty and A. M. Srivastava, Nucl. Phys. **B406**, 795 (1993).
[33] T. C. Petersen and J. Randrup, Phys. Rev. C **61**, 024906 (2000).
[34] J. Adams *et al.* (STAR Collaboration), J. Phys. G **32**, L37 (2006); J. Putschke, J. Phys. G: Nucl. Part. Phys. **34**, S679 (2007).S. A. Voloshin, Phys. Lett. B **632**, 490 (2006); A. Dumitru, F. Gelis, L. McLerran, and R. Venugopalan, Nucl. Phys. **A810**, 91 (2008).
[35] A. Atreya, A. Sarkar, and A. M. Srivastava, Phys. Rev. D **85**, 014009 (2012).